PNAS

Supporting Information for

Spontaneous dark formation of OH radicals at the interface of aqueous atmospheric droplets

Kangwei Li[1,a], Yunlong Guo[1,2], Sergey A. Nizkorodov[3], Yinon Rudich[4], Maria Angelaki[1], Xinke Wang[3], Taicheng An[2], Sebastien Perrier[1], Christian George[1,*]

[1] Univ Lyon, Université Claude Bernard Lyon 1, CNRS, IRCELYON, F-69626, Villeurbanne, France

[2] Guangdong Key Laboratory of Environmental Catalysis and Health Risk Control, Guangdong-Hong Kong-Macao Joint Laboratory for Contaminants Exposure and Health, Institute of Environmental Health and Pollution Control, Guangdong University of Technology, Guangzhou 510006, China

[3] Department of Chemistry, University of California, Irvine, Irvine, CA 92697, USA

[4] Department of Earth and Planetary Sciences, Weizmann Institute, Rehovot 76100, Israel

[a] Now at: Department of Environmental Sciences, University of Basel, 4056, Basel, Switzerland

*To whom correspondence should be addressed. Email: christian.george@ircelyon.univ-lyon1.fr

This PDF file includes:

Supporting text S1 to S12
Figures S1 to S14
Tables S1 to S2
SI References

Other supporting materials for this manuscript include the following:

Movies S1: A typical experiment showing how the home-built mist chamber is operated in a recirculation mode

Supporting Information Text

Text S1 Chemical materials

All chemicals were used as purchased: disodium terephthalate (TA) (Alfa Aesar, ≥99% purity), 2-hydroxyterephthalic acid (TAOH) (Sigma Aldrich, 97% purity), adipic acid (Fluka, ≥99.5% purity), 2-chloroethanol (Sigma Aldrich, ≥99% purity), 1-butanol (Sigma Aldrich, ≥99.7% purity), cyclohexane (Merck Schuchardt, ≥99% purity), ammonium chloride (Sigma Aldrich, 99.99% purity), ammonium hydrogen sulfate (Acros Organics, 99% purity). The N_2O gas cylinder (1% N_2O in N_2) was purchased from Air Products Inc. The pH of some solutions (usually below 6 or above 7) was adjusted by adding HCl or NaOH, and the solution pH was measured by a Metrohm pH meter (Model 913).

Text S2 TAOH quantification and interference using fluorescence spectrometry

TAOH is a fluorescent compound, and we used a commercial fluorescence spectrometer (RF 6000, Shimadzu) to quantify its concentration. We choose 310 nm as the excitation wavelength, and the emission wavelength is usually scanned from 380 nm to 480 nm at a speed rate of 200 nm min^{-1}, with excitation and emission slit widths set at 5 nm. The data were exported from the software LabSolutions RF 1.17. **Fig. S1** shows typical fluorescence emission spectra of TAOH standards from 0.49 nM to 1000 nM, exhibiting an excellent linearity with the intensity from the emission peak at 422 nm. We performed the calibration with TAOH standards regularly and applied the linear regression for TAOH quantification. The TAOH quantification process is similar to some previous studies that use single wavelength-pair mode (i.e., excitation/emission wavelengths of 323 nm / 435 nm (1), 320 nm / 420 nm (2); 310 nm / 420 nm (3)).

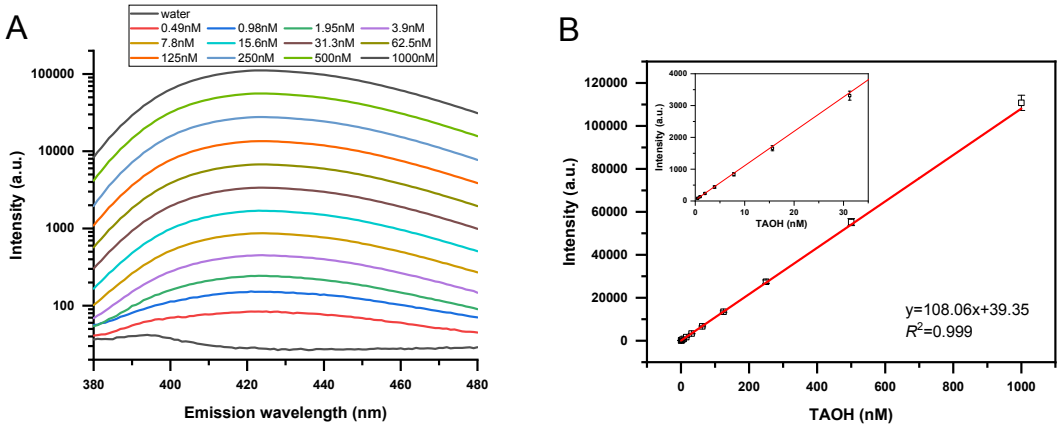

Fig. S1 (A) Fluorescence emission spectra (excited at 310 nm) of TAOH standards from 0.49 nM to 1000 nM. The fluorescence intensity is shown on a logarithmic scale to highlight the wide dynamic range of the measurement. (B) Typical calibration curve for TAOH quantification using fluorescence spectrometry, and the intensity refers to the peak emission wavelength at 422 nm.

Although TA fluoresces much weaker than TAOH does, it may potentially interfere when measuring TA and TAOH mixtures at very low TAOH concentrations. **Fig. S2** shows the fluorescence emission spectra (excited at 310 nm) from TA standards at different solution pH and concentrations. Note that the TA concentration is 4-5 orders of magnitude higher than that of TAOH at the same fluorescence intensity, and it has a very different spectrum, making it easy to distinguish it from TAOH. Higher TA concentrations result in higher fluorescence emission signal, as expected, while the interference from pH becomes more significant when TA solution pH is below 5. Therefore, we choose 0.05 mM TA at pH=6.2 for the mist chamber experiments (**Fig. 1B**), and 0.1 mM TA for the flat surface experiments (**Fig. S3** and **Text S3**), minimizing the interference due to the presence of TA.

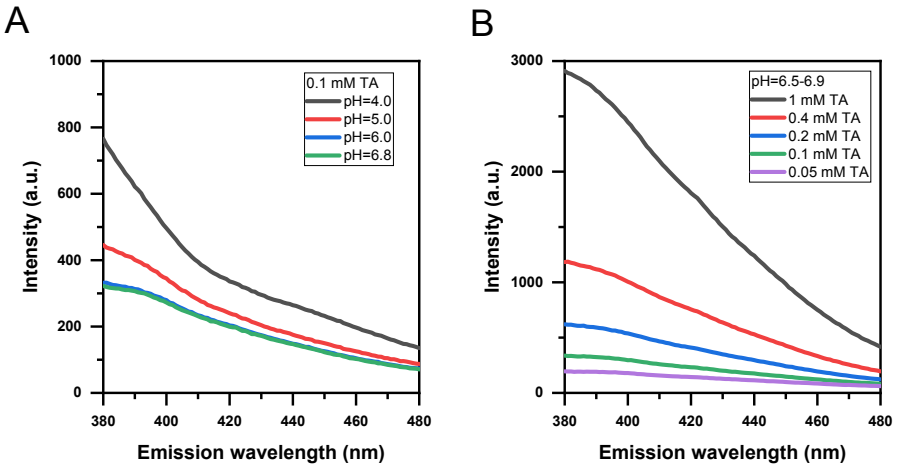

Fig. S2 Fluorescence interference from TA standards at different (A) solution pH and (B) TA concentrations.

Text S3 Interfacial $OH_{(aq)}$ formation from flat surface of macroscopic bulk water

We performed a set of simple experiments to confirm whether OH radical can be spontaneously formed at the interface of bulk water at a macroscopic scale. As shown in **Fig. S3A**, a 60 mL glass bottle was fully filled with 0.1 mM TA bulk solution that O_2 was degassed in prior, leaving no headspace or interface with the air, while another same-sized glass bottle was filled with a small volume of the same TA solution (3 mL). The first sample should not have any major contributions from the air-water interfacial chemistry, whereas the second sample has an area of ca. 8.3 cm^2 exposed to air, and a reduced volume of bulk solution, thus enhancing the effects of the air-water interfacial chemistry. Every 3-5 days, we transferred the liquid solution from these bottles into a quartz cuvette for fluorescence measurement, and then transferred back to the original bottles to continue the flat surface experiment, and no dilution effect was accounted during the whole process. **Fig. S3B** shows time-dependent TAOH fluorescence emission spectra of bulk and interfacial solutions under acidic and nearly neutral conditions, with pH values ranging from 4.0 to

6.8. Compared with the full bulk solutions, the interfacial result clearly shows significant formation of TAOH at all pH, with the TAOH concentrations accumulating over time.

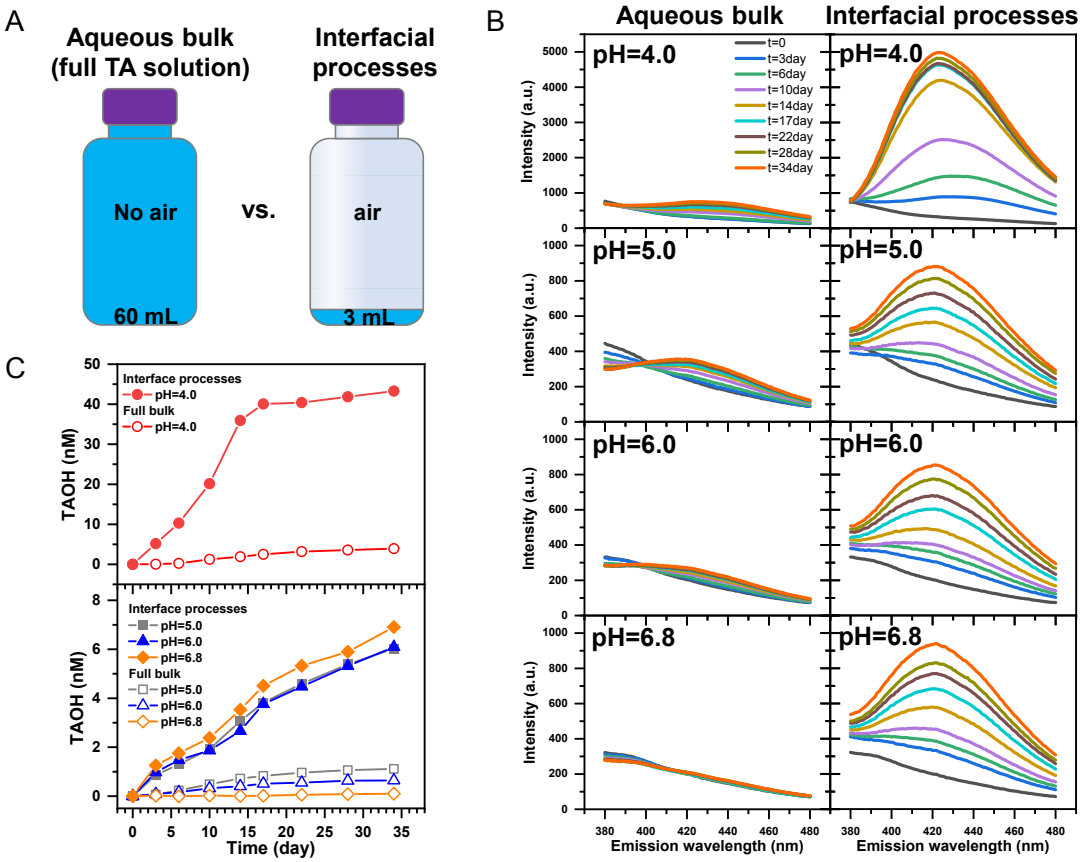

Fig. S3 Confirmation of $OH_{(aq)}$ production at the air-water interface in the macroscopic scale. (A) Schematic of two glass bottles (60 mL size), filled with 60 mL and 3 mL TA solution to represent conditions dominated by bulk and interfacial reactions, respectively. (B) Time-dependent fluorescence emission spectra (excited at 310 nm) measured from glass bottles providing bulk and interfacial results, with 0.1 mM TA at pH=4.0, 5.0, 6.0, and 6.8. (C) Time-dependent TAOH concentrations quantified from (B)

As shown in **Fig. S3C**, we further quantified time-dependent TAOH concentrations for the above bulk and interfacial solutions under different pH conditions, with a time window of five weeks. As for the interfacial case in pH=4.0 solution, TAOH concentration first increased to 40 nM at a fast production rate of 2.5 nM day^{-1} for the initial 17 days, and then slowly reached 43 nM at a rate of 0.20 nM day^{-1} during the rest of the experimental period. Meanwhile, TAOH concentrations in other interfacial solutions (pH=5.0, 6.0, and 6.8) reached 6−7 nM at a production rate of 0.18−0.20 nM day^{-1} for the whole period, which corresponds to a $OH_{(aq)}$ production flux of 0.57−0.63 nM day^{-1}, assuming TAOH production yield of 0.315 (3). The reason for the contrast rates of two periods in interfacial pH=4.0 solution remains unclear. Nevertheless, these experiments clearly confirm that

the interfacial production of OH radicals is a general phenomenon, which can be observed at a macroscopic scale of air-water interface when there is enough low detection limit and long duration time.

Text S4 Producing TA-containing microdroplet from mist chamber

Fig. 1B shows the schematic of the home-built mist chamber, which is made of glass with a total volume of ~110 mL, in which the solution liquid was lifted up due to pressure difference after gas flow entering, and droplets were produced by spraying aqueous bulk solutions. A 47 mm hydrophobic PTFE membrane filter (0.2 μm pore size, Ref: FGLP04700, Merck Millipore Ltd) was connected before the flow output (at the top of the mist chamber), which only allowed gas flow passing through, while microdroplets were hindered by the PTFE membrane, and dropped back into the bulk solution (see **Movie S1** for the typical operation of mist chamber experiment). We tested the membrane filter by connecting a condensation particle counter (CPC, TSI 3776) at the outlet of mist chamber, and no particle was detected from the output gas flow during the spraying process. For our experimental conditions, we initially added 20 mL bulk TA solution (0.05 mM TA + 2.5 mM NH_4Cl, pH=6.2) into the mist chamber, and used a bubbler to generate humidified gas (i.e., air, N_2, O_2, etc.) as the spraying flow, which was adjusted by mass flow controllers (MFC) at a fixed flow rate of 2.5 L min^{-1}. By maintaining the spraying process and with the droplets being recycled, TAOH in the solution is expected to accumulate overtime if $OH_{(aq)}$ radicals are formed in the microdroplet containing TA.

As shown in **Fig. 1B**, we measured the time-dependent fluorescence emission spectra (excited at 310 nm) of the bulk TA solution during the whole spraying period, and we observed clear TAOH fluorescence signal after 15 or 16 h spraying under five different gases, though the fluorescence intensity is different among them. When adding chloroethanol to the gas flow, humidified N_2 flow passed through the headspace of a 120 mL bottle that was filled with 30 mL pure 2-chloroethanol solution, and carried the gaseous chloroethanol vapor as the spraying gas into the mist chamber. The chloroethanol concentration in N_2 is estimated as 0.72% based on its vapor pressure. We note that the peak wavelength of TAOH fluorescence emission spectra has a small shift to ~440 nm in the chloroethanol experiment (**Fig. 1B**), which is likely due to the interference from chloroethanol as it can be partially dissolved in the solution water in the mist chamber during the spraying and droplet recycling process.

Note that the bulk solution in the mist chamber was also evaporating due to the spraying flow, resulting in more concentrated TA and hence the observed shift in the baseline, as a higher TA concentration may cause larger fluorescence interference (see **Fig. S2** and **Text S2** for details). In our mist chamber experiments, usually 75−90% of the solution water was evaporated after 15 h spraying (with remaining liquid volume of 2−5 mL), corresponding to a liquid loss rate at 1.0−1.2 mL h^{-1}, and resulting in an exponentially increase of TAOH concentration overtime (**Fig. 1B** and

Fig. S4A). Nevertheless, the water evaporating and TA concentrating process in the mist chamber would not have much influence on TAOH confirmation and quantification after 15 or 16 h spraying, as TA concentration is expected to increase up to a factor of 5−10. According to liquid loss rate for each mist chamber experiment, we estimated time-dependent remaining liquid volume and TA concentration. With TA fluorescence signal at 422 nm from different TA concentrations (**Fig. S2B**), we can subtract the background interference from TA. We finally calculate background-corrected time-dependent TAOH concentration and its molar amount (in nmol). As shown in **Fig. S4**, TAOH molar amount showed less non-linearity as a function of time than TAOH concentration, though both metrics represented the production flux of OH radical through mist chamber experiments. Compared with the pure N_2 condition, we observed enhanced TAOH formation for experiments using N_2O or chloroethanol as spraying gas, suggesting that the role of N_2O and chloroethanol as electron scavenger was taking place.

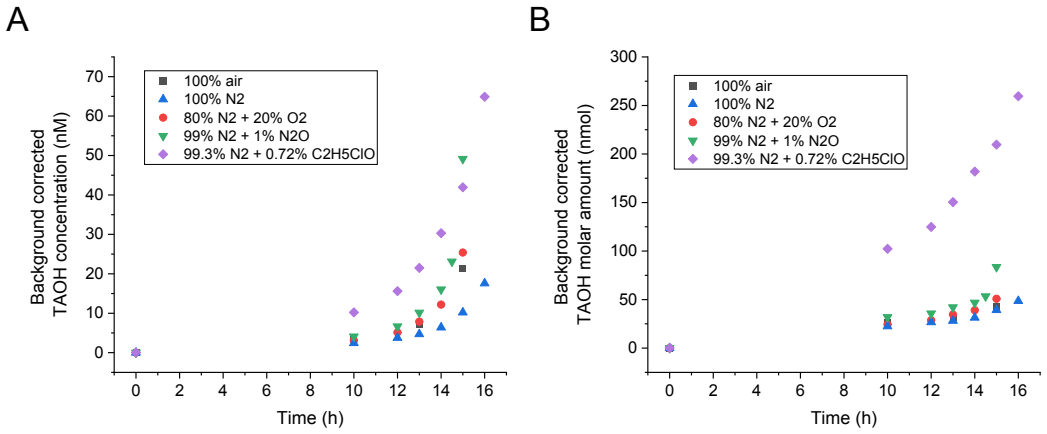

Fig. S4 Background-corrected (A) TAOH concentration and (B) its molar amount as a function of time for the five mist chamber experiments.

Text S5 Producing TA-containing microdroplet from a commercial atomizer

To test whether our observations are dependent on the spraying procedure, we also used a commercial atomizer (TSI 3076) to atomize bulk TA solution (25 mM NH_4Cl + 1 mM TA) to generate polydisperse aerosol droplets, with droplet sizes ranging from a few tens of nanometers to microns. As shown in **Fig. S5A**, the microdroplets were continuously impacted and collected as condensing liquid in 1 or 3 clean glass vessels (5 L) directly connected to the atomizer output, and then we transferred the liquid into a quartz cuvette for fluorescence analysis. Note that these atomizing experiments usually last for several hours, which makes it possible to accumulate enough condensing liquid volume in glass vessels that can be transferred into a quartz cuvette for fluorescence analysis. By using an Aerodynamic Particle Sizer (APS, TSI 3321), those large droplets produced from the atomizer showed slightly different size distribution depending on where the measurement was taken, but generally peaked at 1.5−3 μm with a broad size range (**Fig. S5B**).

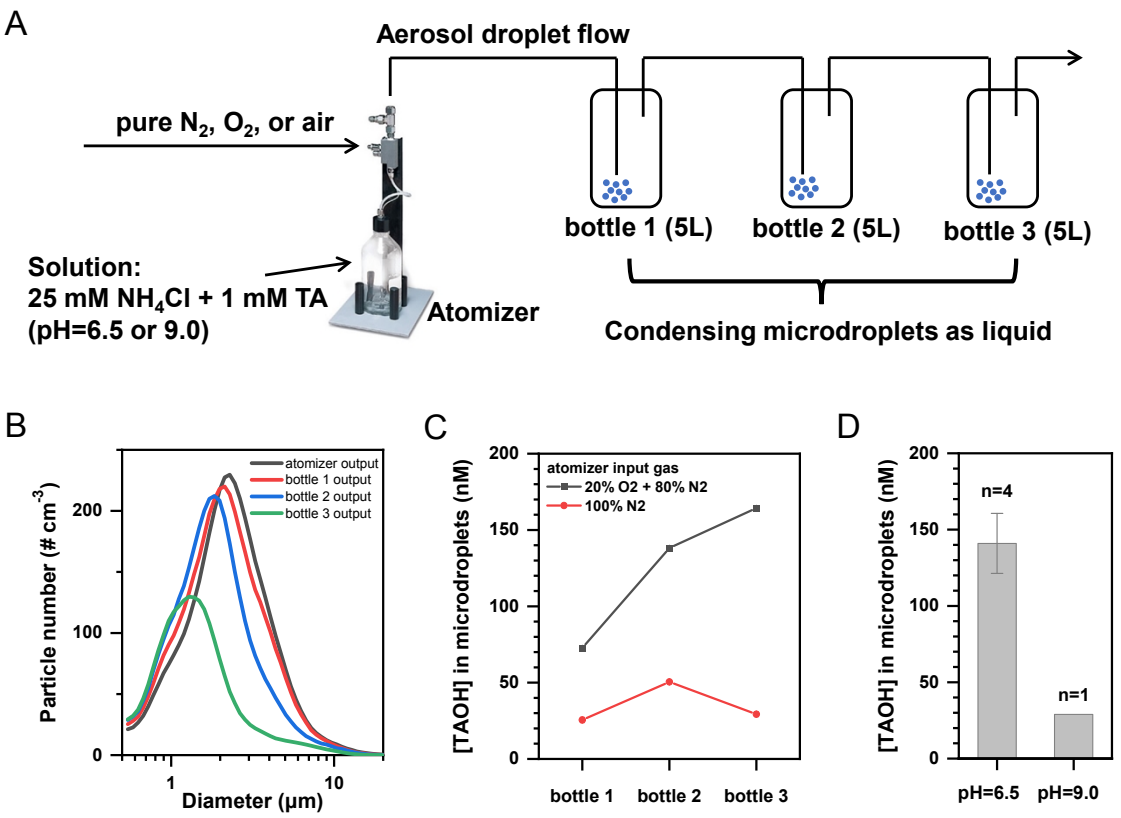

Fig. S5 Confirmation of $OH_{(aq)}$ production at the air-water interface of microdroplets produced from an atomizer. (A) Setup for producing aerosol droplets from 25 mM NH_4Cl + 1 mM TA solution with different input gas (pure N_2, O_2, or air). (B) The size distribution of large droplets measured from the output of atomizer or condensing bottles. (C) Measured TAOH concentrations for microdroplets produced by atomizing 25 mM NH_4Cl + 1 mM TA solution (pH=6.5) with different carrier gases (100% N_2 vs. 80% N_2 + 20% O_2), collected as condensing liquid in the three tandem bottles as shown in (A). (D) Measured TAOH concentrations for microdroplets by atomizing 25 mM NH_4Cl + 1 mM TA solution at different pH (pH=6.5 or 9.0) with pressurized pure air of ~3 bar (~3.5 L min^{-1}) as input gas, which was collected in one single 5 L glass vessel connected to atomizer output.

We first atomized 25 mM NH_4Cl + 1 mM TA solution (pH=6.5) using different carrier gases (100% N_2 vs. 80% N_2 + 20% O_2), with a total gas flow of 3 L min^{-1} controlled by mass flow controllers (MFC), leading to an average residence time of aerosol droplets travelling through each glass bottle of ca. 100 s. We observed TAOH fluorescence signals in those microdroplets collected from different bottles under the two gas flow conditions mentioned above, with quantified TAOH concentrations shown in **Fig. S5C**. The TAOH concentrations in microdroplets generally showed an increasing trend with increasing residence time, except the bottle 3 under 100% N_2 condition, which might be due to the changed droplet size distribution in this case. Nevertheless, the production of TAOH was enhanced by a factor of 3−5 in the presence of 20% O_2, compared to pure

N_2 condition. This is in good agreement with the mist chamber experiments (**Fig. 1B**), and further demonstrates the important role of O_2 in interfacial $OH_{(aq)}$ production.

Fig. S5D also shows that the TAOH concentrations in microdroplets are pH-dependent i.e., 141 ± 20 nM (n=4; pH=6.5) and 29 nM (n=1; pH=9.0) respectively, suggesting that the interfacial $OH_{(aq)}$ production might be more efficient under acid than alkaline condition. For this specific case, the atomizer output flow rate was measured at ~3.5 L min^{-1} under ~3 bar regulated pure air, providing an average residence time of ~86 s for those microdroplets in 5 L glass vessel. This yields a TAOH production rate of 1.64 ± 0.23 nM s^{-1}, and hence an $OH_{(aq)}$ production rate of ca. 5.2 ± 0.7 nM s^{-1} for microdroplets with average diameter of 2.6 μm at pH=6.5.

Text S6 Aerosol droplet filter collection in chamber experiments and its extraction

The setup for chamber experiment is shown in **Fig. S6**, where chamber aerosol droplets were collected onto a 47 mm quartz filter through a particle sampler, with a known sampling flow rate and duration. **Fig. S7-S8** show the evolution of particle concentration and size distribution from three typical chamber experiments, marked with aerosol droplet injecting and filter sampling periods. After collecting chamber aerosols onto the filters, we first cut the full filter into small pieces, and then transferred into a vial (30 mL size) with 5 mL water (Optima® LC/MS grade, Fisher Scientific Inc.), which was then agitated for 60 min using an orbital shaker at 1000 rpm. After that, the extracts were filtered through a syringe on a 0.2 μm PTFE membrane (13 mm, product ID: 4552T, Pall Corporation) to remove insoluble materials. The whole filter extraction and filtration process was completed within 24 h. Because high-frequency ultrasound can produce $OH_{(aq)}$ radical in the solution (4), we did not use any sonication during the filter extraction. The extracted liquid amount was usually 4.1−4.5 mL, which was then used for fluorescence analysis, and some samples were also analyzed with offline liquid chromatography (see **Text S7**). Based on the above procedures, we examined the filter extraction efficiency by adding known amount of TAOH standards onto the clean filters. **Fig. S9** shows reasonably good performance for the filter extraction efficiency, which was calculated based on added molar amount and extracted molar amount of TAOH (measured TAOH concentration multiplying extracted liquid volume), with an average of ~90% from six trials.

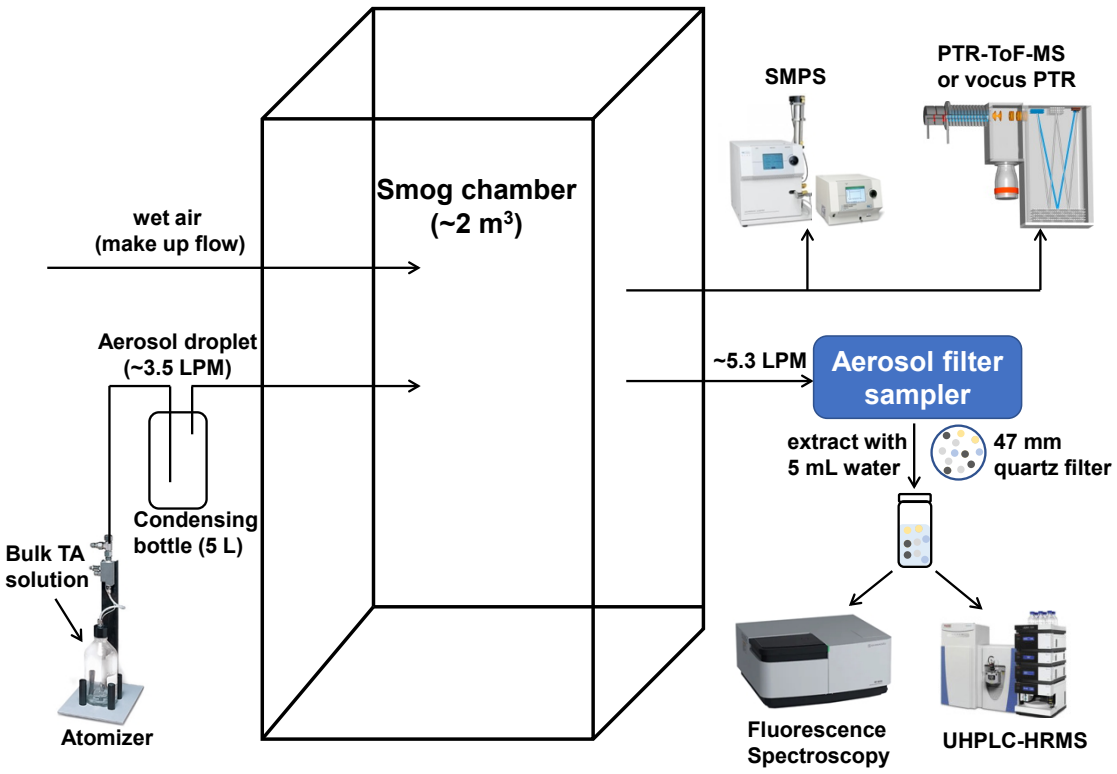

222

223 **Fig. S6** Schematic of the setup for chamber experiments. All the chamber experiments were
224 performed under high humidity (~76%) and room temperature (~23℃) condition.

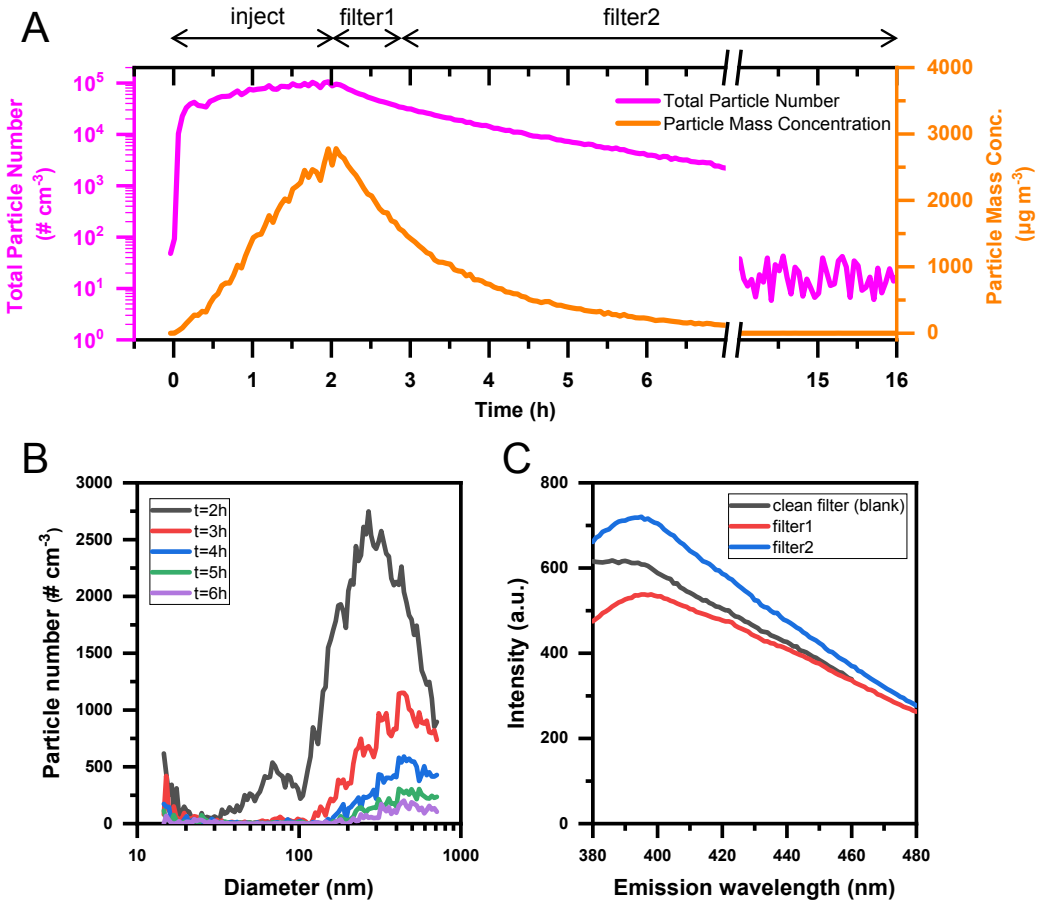

225

226 **Fig. S7** A blank chamber experiment performed after a typical TA chamber experiment the next
227 day, in which only NH_4Cl droplets were injected (atomizing 25 mM NH_4Cl solution). (A) Time series
228 of total particle number and mass concentration (assuming density 1 g cm^{-3}), with periods for
229 aerosol injection and sampling of two filters. (B) Time-dependent particle number size distribution
230 from SMPS measurement. (C) Fluorescence emission spectra (excited at 310 nm) measured for
231 the two filters collected with chamber droplets and one clean blank filter (no aerosol loading) after
232 water extraction.

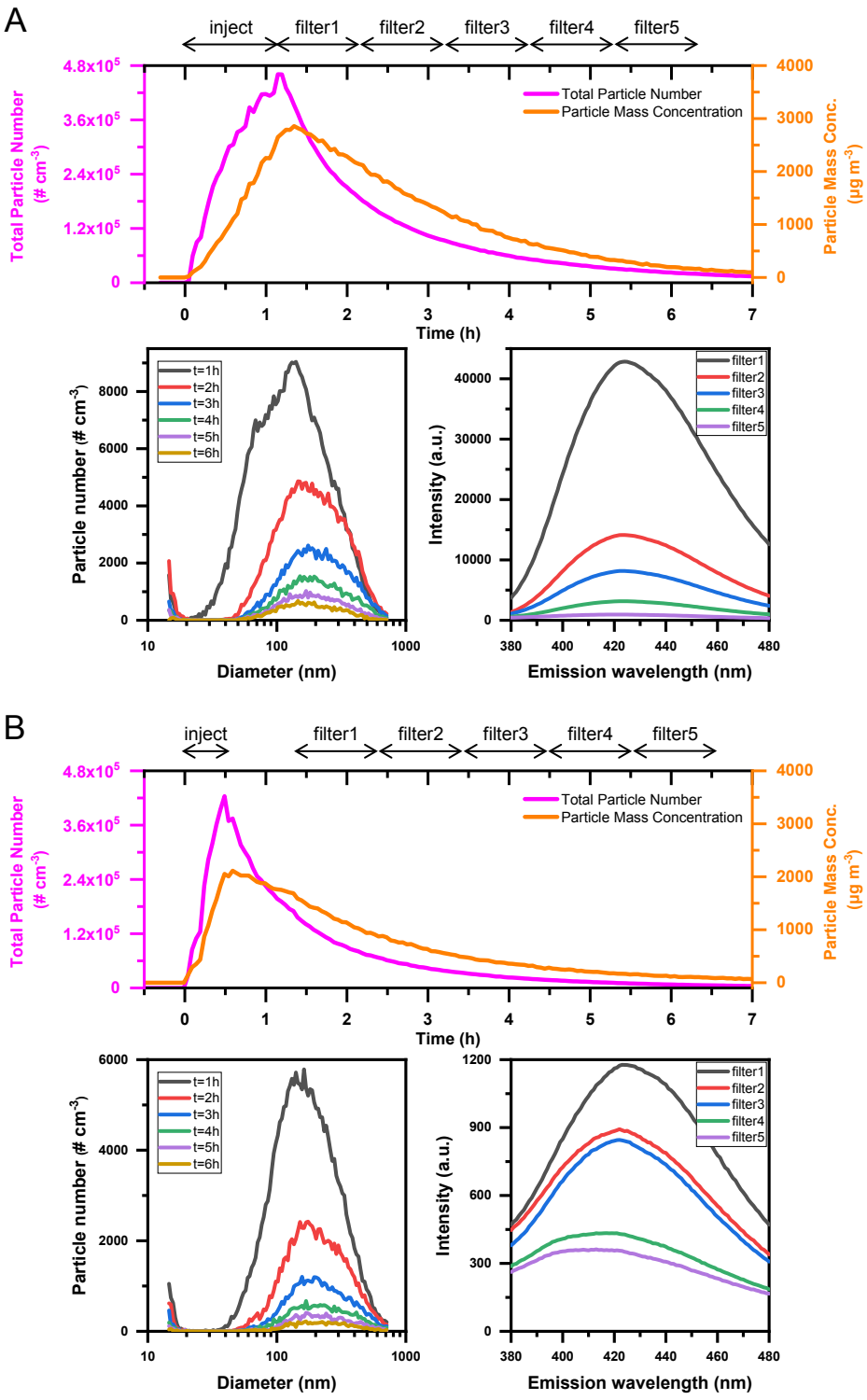

Fig. S8 Same as Fig. S7. (A) A typical chamber experiment (E2) where TA-containing droplets were injected (atomizing 25 mM NH_4Cl + 1 mM TA). (B) A typical chamber experiment (E7) that injecting aerosol droplets containing both TA and adipic acid (atomizing 25 mM NH_4Cl + 1 mM TA + 10 mM adipic acid).

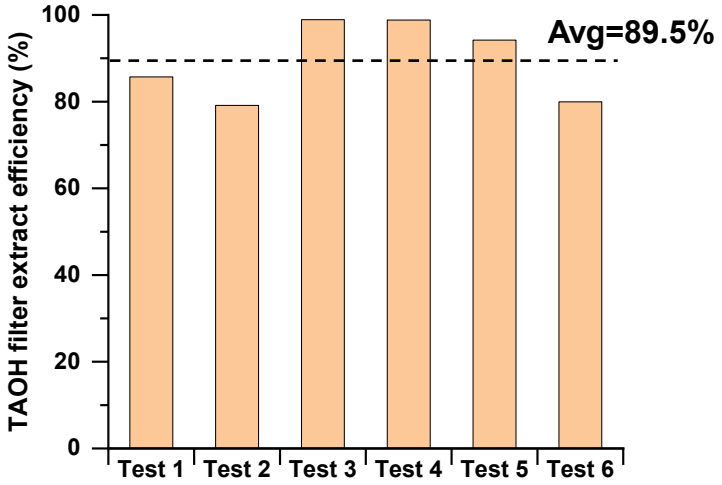

Fig. S9 Filter extraction efficiency for TAOH by adding known amount of TAOH standards onto filters.

Text S7 Offline liquid chromatography measurements

In order to complement the offline fluorescence measurements, some filter extracts were also analyzed by an ultra-high-performance liquid chromatography (UHPLC, Dionex Ultimate 3000, Thermo Scientific) coupled with high-resolution mass spectrometry (HRMS, Q-Exactive Hybrid Quadrupole-Orbitrap mass spectrometer, Thermo Scientific). HRMS was equipped with a heated electrospray ionization source (ESI), and spray voltage of −2.6 and 3.2 kV were applied for negative (−) and positive (+) ionization mode, respectively. The mass resolving power was 140,000 at *m*/*z* = 200, with the scanning range setting as *m*/*z* 50−750. External mass calibration for HRMS was performed on a daily basis using a 2 mM sodium acetate solution, which can provide a series of negative and positive adduct ions (with known *m*/*z*) in the range of *m*/*z* 50–750. The external mass calibration was completed until the error was below 0.5 ppm.

The filter extracts from some chamber experiments (E1, E2, E3, E6, E7; see **Table S1** for detailed description of experiment ID), TAOH standards (10 nM, 100 nM, 1000 nM), TA standards (0.1 μM - 100 μM) and water blank were injected for UHPLC-HRMS analysis, and the injection volume was 5 μL. Analytes were separated using a Waters Acquity HSS C18 column (1.8 μm, 100 × 2.1 mm). The mobile phases were (A) 0.1% formic acid in water (Optima® LC/MS grade, Fisher Scientific Inc.) and (B) 0.1% formic acid in acetonitrile (Optima® LC/MS grade, Fisher Scientific Inc.). The gradient elution procedure used in this study is the same as that in our previous studies (5). Briefly, gradient elution was performed by the A/B mixture at a total flow rate of 0.3 mL min^{-1} for 22 min: 0−2 min at 1% B, 2−13 min with a linear gradient to 100% B, 13−15 min held at 100% B, 15.0−15.1 back to initial condition at 1% B, 15.1−22 min stabilized at 1% B.

Based on UHPLC-HRMS measurement from the TAOH standards (**Fig. S10A, C, E**), we quantified TAOH concentrations for filter extracts from some chamber experiments (E1, E2, E3, E6, E7), and overall good correlation was found between UHPLC-HRMS and fluorescence measurement (**Fig. S10G**). Similarly, we measured TA standards at different concentrations and established calibration curve for TA standards (**Fig. S10B, D, F**), which enables to further quantify TA concentration from filter extracts. Good correlation (R^2=0.92) was also found between TA concentration in filters extracts and average chamber aerosol concentration during the corresponding filter sampling period (**Fig. S10D**), which is an expected result. This also indicates the robustness of our experiment procedures (e.g. generating TA-containing aerosol droplets, chamber measurement and filter sampling/extracting method) between different experiment runs. We notice that both TA and TAOH co-eluted at ~6.50 min under our LC conditions. However, this does not lead to misidentification due to the ultra-high resolving power of the mass spectrometer used (**Fig. S10A-D**). **Fig. S11-S12** show the chromatogram for selected ions from filter extracts (E6 and E7) with a mass tolerance of 10 ppm, and the data were processed and exported using the Xcalibur 2.2 software (Thermo Scientific).

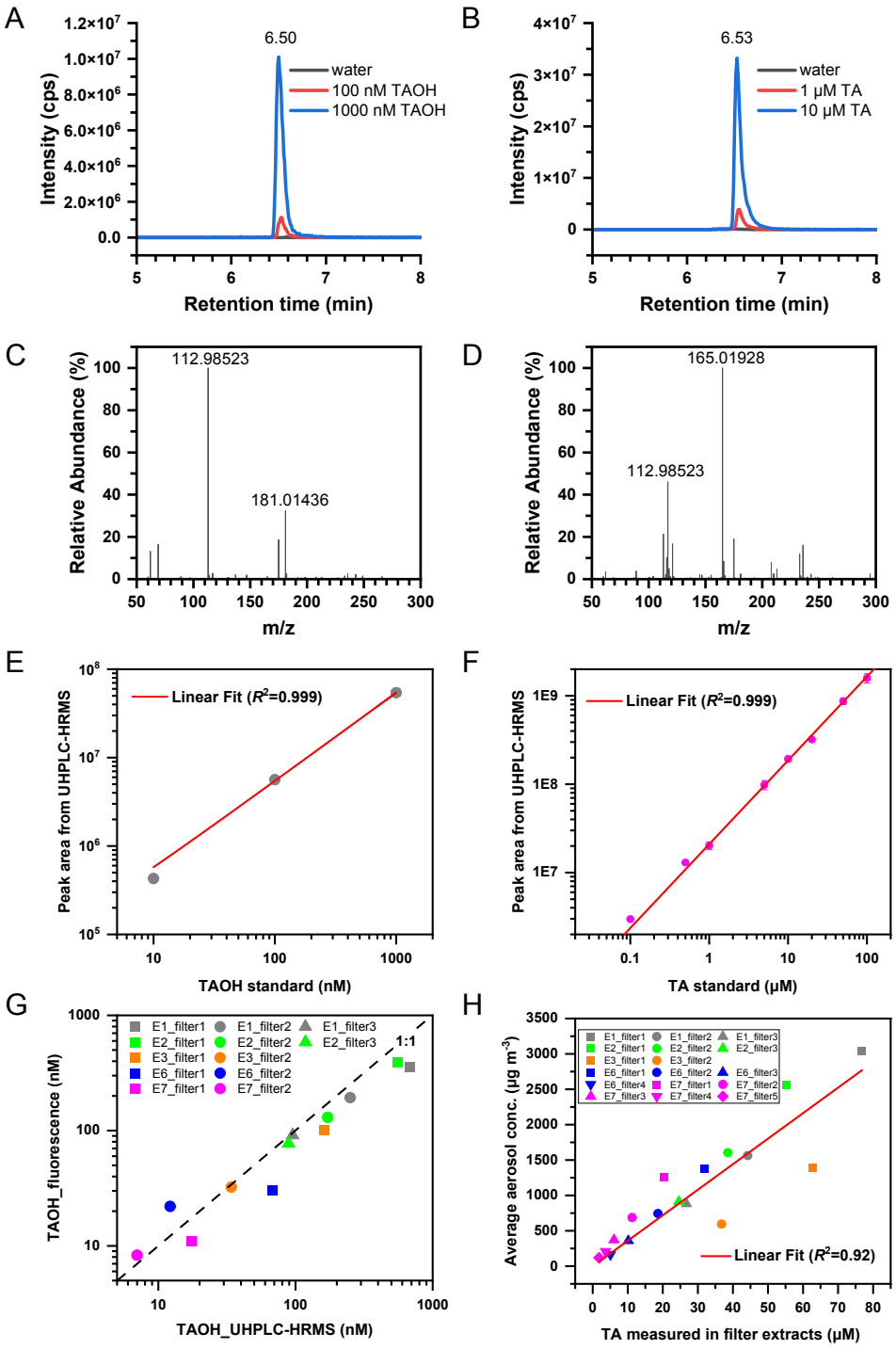

277

278 **Fig. S10** Extracted ion chromatograms (EIC) for (A) TAOH standards (*m/z* = 181.01425) and (B)
279 TA standards (*m/z* = 165.01933), with a mass tolerance of 10 ppm. Mass spectra for (C) 1000 nM
280 TAOH and (D) 10 μM TA eluting at ~6.50 min. Calibration curve for (E) TAOH standards (10 nM,
281 100 nM and 1000 nM) and (F) TA standards (0.1 μM - 100 μM) using UHPLC-HRMS. (G)
282 Comparison of quantified TAOH concentrations in selected filter extracts between fluorescence

spectrometry and UHPLC-HRMS. (H) Comparison between quantified TA concentrations in filter extracts and average aerosol concentrations in chamber during filter sampling period (data summarized in **Table S1**). UHPLC-HRMS was operated with a negative ionization mode.

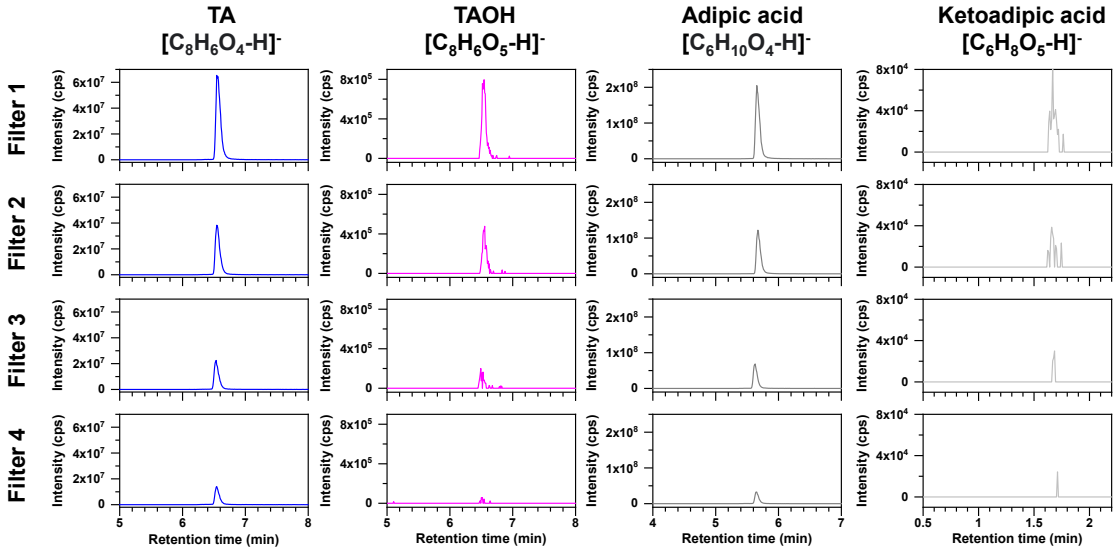

Fig. S11 Offline UHPLC-HRMS chromatogram for the four filter extracts collected from chamber experiment (E6) with a negative ionization mode. The selected *m*/*z* values were 165.01933, 181.01425, 145.05063 and 159.02990 for TA, TAOH, adipic acid and ketoadipic acid, respectively.

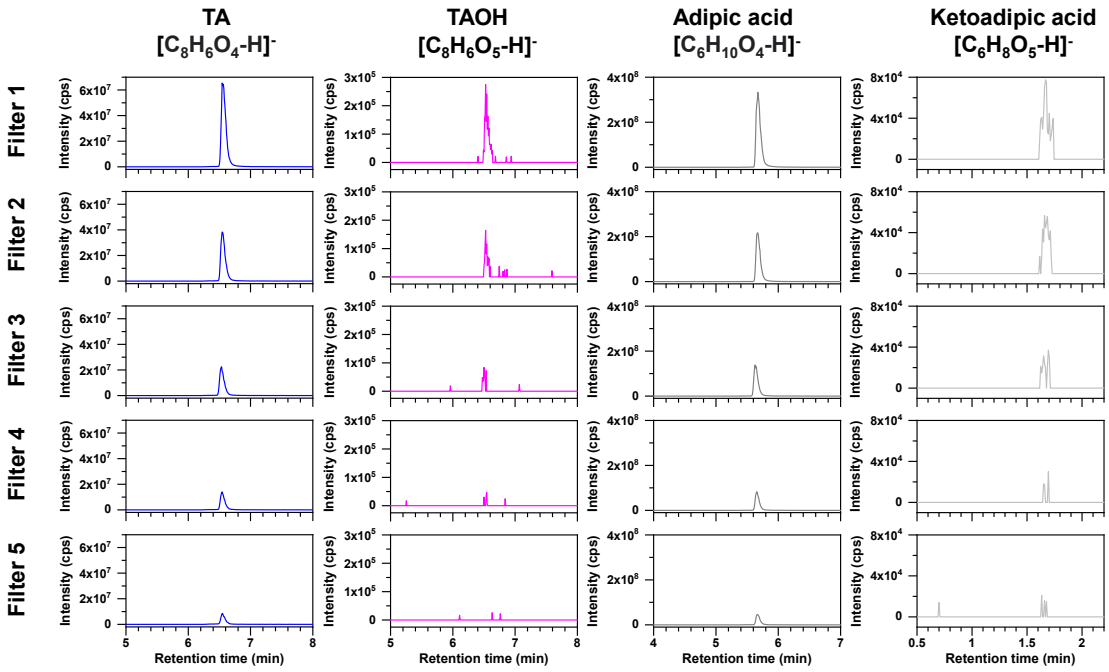

Fig. S12 Same as Fig. S11 but for chamber experiment (E7)

Text S8 Gas-phase analysis by PTR-ToF-MS and Vocus PTR-ToF-MS

Both PTR-ToF-MS (PTR–ToF 8000, Ionicon Analytik GmbH, Inns-bruck, Austria) and Vocus PTR-ToF-MS (Tofwerk AG, Thun, Switzerland) have been widely used to monitor gas-phase species (6). PTR-ToF-MS has the benefit of being a more established instrument, while the newer Vocus PTR-ToF-MS has a much higher sensitivity and lower detection limit (7, 8). Both instruments were operated under H_3O^+ ionization mode. Since the aerosol droplet concentration in the chamber was high, a particle filter was used before the inlet of PTR-ToF-MS instruments to avoid source contamination.

PTR-ToF-MS (PTR–ToF 8000) was employed for E4 and E5 experiments to monitor gas-phase cyclohexane and 1-butanol concentration, with a sampling flow rate of 100 mL min^{-1} through a heated Silicon Steel tube (60 ℃) to minimize adsorption and loss of compounds. The detailed instrument operation and settings were described in our previous studies (9, 10). Briefly, the instrument was set to a drift–tube pressure of 2.2 mbar, drift temperature of 60 ℃, source current of 4 mA, and drift voltage of 520 V, resulting in E/N (electric field strength to number density ratio) of approximately 120 Townsend (Td, 1 Td = 10^{-17} V cm^2). These settings were optimized in order to have less than 5% impurities in the H_3O^+ signal. The raw data were recorded by TofDaq software (Tofwerk AG, Switzerland) and subsequently treated by PTR–MS Viewer 3.2.8. The mass calibration of the spectra was performed via three ions with known mass ($H_3{}^{18}O^+$, *m/z* = 21.0221; NO^+, *m/z* = 29.9974; $C_3H_7O^+$, *m/z* = 59.0491), which were commonly used for internal calibration during data acquisition and post-processing.

Gas phase cyclohexane was added in experiment E4 as the first trial experiment to test if there is $OH_{(g)}$ released from the aerosol droplets. However, no cyclohexane oxidation products were detected by PTR-ToF-MS in this experiment. This is probably due to the 1) low detection sensitivity for this version of PTR instrument; 2) the existence of TA in the aqueous phase that limits the release of $OH_{(g)}$; 3) large chamber dilution effect as ~10 L min^{-1} humidified clean air was supplied to offset the particle filter sampling flow in experiment E4. Therefore, Vocus PTR-ToF-MS was employed in two additional experiments (E11 and E12) to monitor cyclohexane and its oxidation products by taking advantage of its high sensitivity and low detection limit, and humidified clean air with minimum flow rate at ~3.5 L min^{-1} was supplied in these two experiments to minimize the chamber dilution effect. In addition, Vocus PTR-ToF-MS did not show dependence of the sensitivity with the high-water mixing ratio of samples (7), which is another advantage for Vocus PTR-ToF-MS as all our chamber experiments were conducted under high RH conditions. More details about the Vocus PTR-ToF-MS are well described in previous literatures (7, 8). In this work, we operated the Vocus ionization source at a pressure of 2.0 mbar, and the raw mass spectra were recorded at a time resolution of 5 s. The raw mass spectra were averaged over 1 min and then analyzed by the software package “Tofware V3.2.3” (https://www.tofwerk.com/software/tofware/) under Igor Pro

7.08 environment (WaveMetrics, OR, USA). Tofware software enables mass calibration and molecular formula assignment, and isobaric ions can be clearly separated through high-resolution analysis. **Fig. S13** shows examples of peak identification for cyclohexane ($C_6H_{13}^+$), cyclohexanone ($C_6H_{11}O^+$) and cyclohexanol ($C_6H_{13}O^+$) measured by Vocus PTR-ToF-MS.

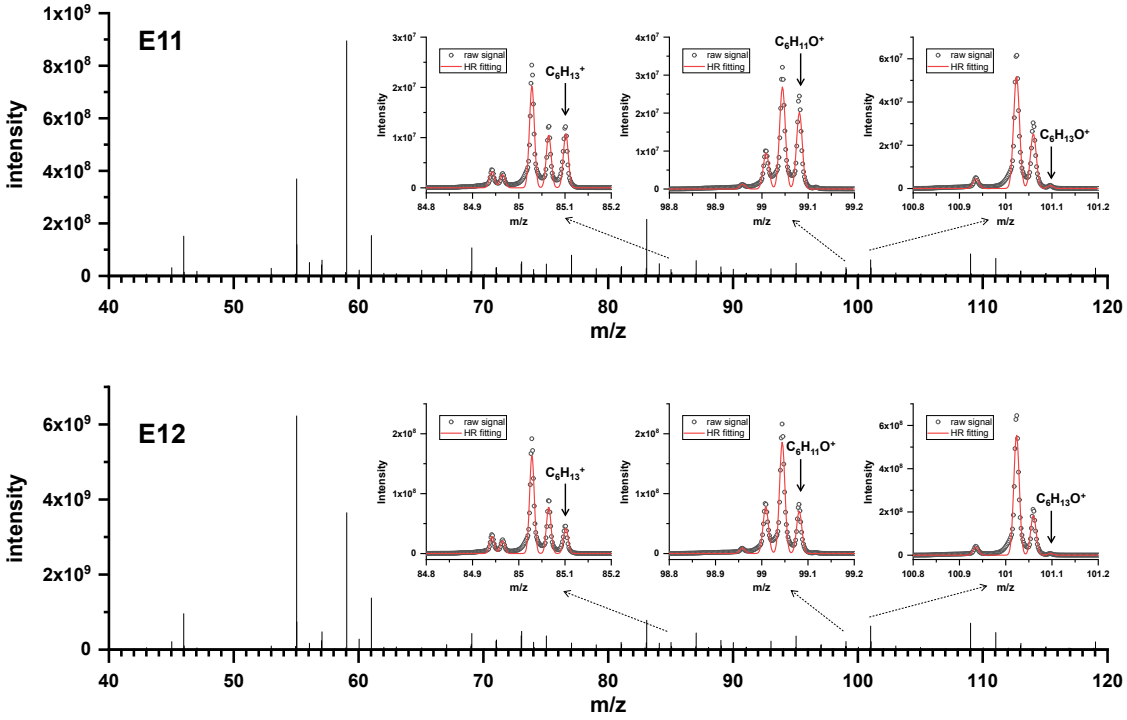

Fig. S13 Full mass spectra and peak identification (insert) for cyclohexane ($C_6H_{13}^+$, *m/z* = 85.1017), cyclohexanone ($C_6H_{11}O^+$, *m/z* = 99.0810) and cyclohexanol ($C_6H_{13}O^+$, *m/z* = 101.0966) measured by Vocus PTR-ToF-MS from two chamber experiments (E11 and E12)

Text S9 Chamber experiments with cyclohexane oxidation products

In order to examine whether interfacial OH radical can induce oxidation chemistry for gas-phase compounds, we performed two additional chamber experiments (E11 and E12; **Table S2**) by injecting only cyclohexane and aerosol droplets (i.e., without TA in solution) into the chamber, and the gas-phase species were monitored by means of the Vocus PTR-ToF-MS instrument (**Text S8**). In experiment E12 (**Fig. 3**), we first injected ~1.1 ppm cyclohexane whose concentration decreased over time due to the dilution effect, as ~3.5 L min^{-1} humidified air flow was continuously supplied into the chamber. Subsequently, we atomized bulk solution (25 mM NH_4HSO_4, pH=1.85) and introduced aerosol droplet into the chamber, and we observed an immediate increase of both cyclohexanone and cyclohexanol. Note that the above processes in experiment E12 were under dark conditions precluding any photooxidation of cyclohexane.

Fig. S14 shows another related chamber experiment (E11; see **Table S2**) where we injected ~0.56 ppm cyclohexane and NH_4HSO_4 aerosol droplets, but under both dark condition and UV irradiation separately. We observed the increase of both cyclohexanone and cyclohexanol signals when switching on UV irradiation, regardless of presence of aerosol droplet or not. This is an expected result because there is always gas-phase OH radical formation due to the photolysis of chamber background photochemical reactive compounds, and it also indicates that our peak assignment for these compounds (as shown in **Fig. S13**) was properly treated. More importantly, after injecting aerosol droplets in the dark, the cyclohexanol signal increased immediately, while the variation of cyclohexanone was not clear compared with the experiment E12 observed in **Fig. 3**, which is likely due to lower reaction rate as less cyclohexane was injected in E11. Both E11 and E12 experiments confirmed the formation of cyclohexane oxidation products after adding NH_4HSO_4 aerosol droplet, suggesting that the interfacial produced OH radical can indeed induce some oxidation chemistry for gas-phase species.

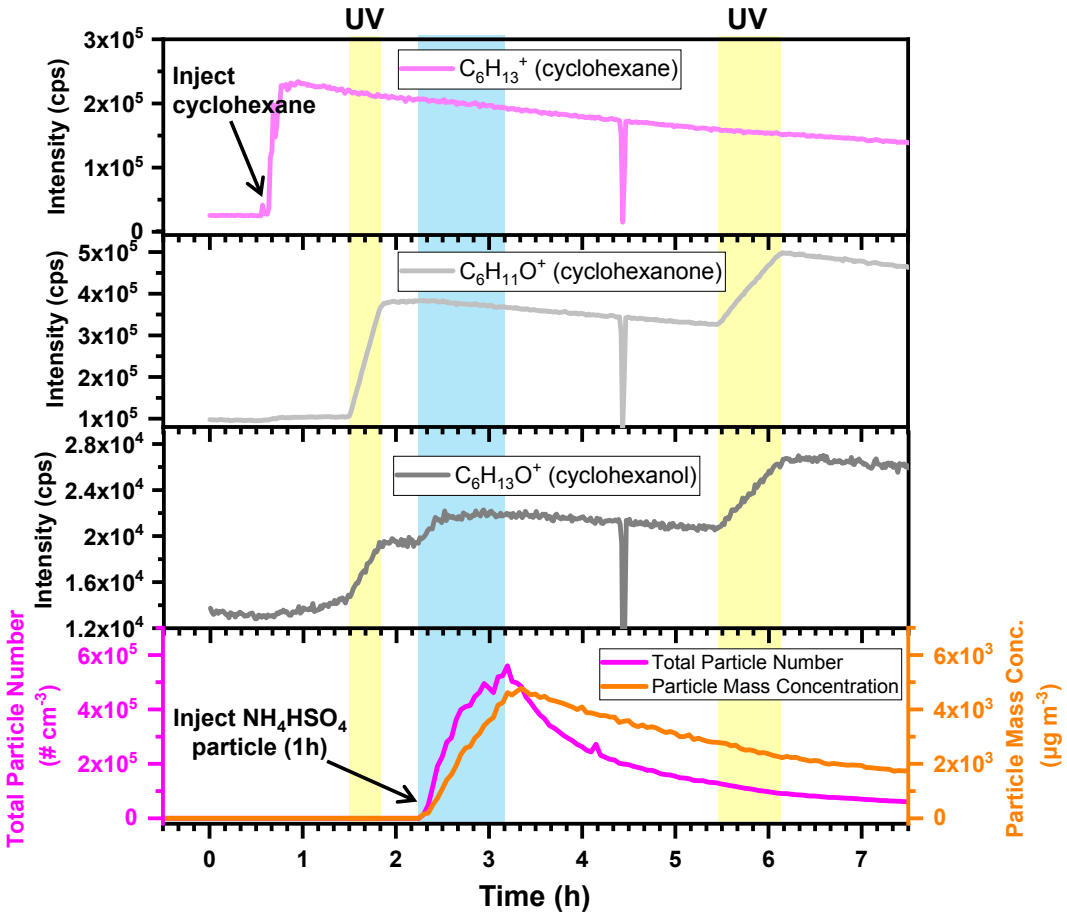

Fig. S14 A chamber experiment similar in Fig. 3 but at ~0.56 ppm cyclohexane and aerosol droplet (NH_4HSO_4) under both dark and UV irradiation conditions (E11 in **Table S2**).

Text S10 Calculation of TAOH and TA concentration in submicron aerosol droplet as well as TAOH production rate

By combining SMPS measurements for the chamber aerosol droplet and fluorescence measurement for filter extracts, we derived the TAOH concentration and its production rate in submicron aerosol droplet for each filter in chamber experiments. The calculation formulas are shown in below:

$$[\mathrm{TAOH}_{\text{ in aerosol}}] = \frac{\text{moles TAOH}}{\text{total aerosol volume}} = \frac{[\mathrm{TAOH}_{\mathrm{meas}}] \times \mathrm{extract}_{\mathrm{vol}} / f_{\mathrm{eff}}}{\mathrm{PM}_{\mathrm{vol}} \times \mathrm{air}_{\mathrm{vol}}} \quad (1)$$

$$\text{Residence time}_{\mathrm{avg}} = \frac{1}{2} \times t_{\text{aerosol injecting}} + t_{\text{aerosol suspending}} + \frac{1}{2} \times t_{\text{aerosol sampling}} \quad (2)$$

$$P(\mathrm{TAOH}) = \frac{[\mathrm{TAOH}_{\text{in aerosol}}]}{\text{Residence time}_{\mathrm{avg}}} \quad (3)$$

Specifically, [$TAOH_{in\ aerosol}$] was determined by the ratio of the TAOH molar amount on the filter (in nmol) and total aerosol volume retained by the filter. TAOH molar amount was determined from measured TAOH concentration from the filter extract ([$TAOH_{meas}$], in nM), the liquid volume from the filter extract ($extract_{vol}$, usually 4.1−4.5 mL), and the filter extraction efficiency factor (f_{eff}) of 0.9 as our best estimate to consider the TAOH lost during the filter extraction (see **Text S6**). Total aerosol volume was determined from average particulate matter (PM) volume concentration during filter sampling period (PM_{vol}, in $\mu m^3\ cm^{-3}$) multiplying the total sampling air volume (air_{vol}, usually 0.318 m^3; see **Materials and methods**).

The average residence time for the aerosol that was sampled onto the filter is a combination of half aerosol injecting period, full aerosol suspending period and half aerosol sampling period. The TAOH production rate (P(TAOH)) was calculated from the ratio of [$TAOH_{in\ aerosol}$] and the average residence time. As mentioned in **Text S7**, we quantified TA concentrations for some filter extracts ([TA_{meas}]) using UHPLC-HRMS, and then we used the same way to derive TA concentration in submicron aerosol droplet ([$TA_{in\ aerosol}$]). **Table S1** summarizes the average residence time, PM mass concentration (converted from PM_{vol} by assuming the aerosol density as 1 g cm^{-3}), [$TAOH_{meas}$], [$TAOH_{in\ aerosol}$], P(TAOH), [TA_{meas}] and [$TA_{in\ aerosol}$] for each filter calculated with above Equations.

Text S11 Calculation of $OH_{(aq)}$ uptake rates from gas-phase

According to literature (11, 12), the uptake rate (R_{uptake}) of OH radicals from gas-phase to droplet can be theoretically calculated from steady state $OH_{(g)}$ concentration and mass transfer coefficient (k_{mt}, in s^{-1}):

$$R_{\mathrm{uptake}} = k_{\mathrm{mt}} \times \mathrm{OH}_{(\mathrm{g})} = \left(\frac{r_{\mathrm{d}}^2}{3D_{\mathrm{g}}} + \frac{r_{\mathrm{d}}}{3\alpha} \sqrt{\frac{2\pi M_{\mathrm{g}}}{RT}} \right)^{-1} \times \mathrm{OH}_{(\mathrm{g})} \quad (4)$$

where r_d is the droplet radius, R is the gas constant (8.314 m^3 Pa mol^{-1} K^{-1}, 1 Pa=1 kg m^{-1} s^{-2}), T is absolute temperature (296 K), M_g is the molecular weight (0.017 kg mol^{-1} for OH radical), and D_g is the gas-phase diffusion coefficient (in m^2 s^{-1}). α is the mass accommodation coefficient ($\alpha \leq 1$), which represents the probability of a vapor molecule that hits the droplet interface to be transferred into the condensed phase.

Both the gas-phase diffusion and mass accommodation are taken into account in the mass transfer coefficient (k_{mt}). We adapted 2.17 ×10^{-5} m^2 s^{-1} as D_g for OH radical, which was experimentally determined in previous literature (13). According to the IUPAC Task Group on Atmospheric Chemical Kinetic Data Evaluation (Data Sheet VI.A1.17 HET_H2OL_17; https://iupac-aeris.ipsl.fr/), the α value for OH radical ($OH_{(g)}$ + $H_2O_{(l)}$) is generally ranging from 0.1 to 1 but not yet satisfactorily determined, thus we assume α values of 0.1, 0.5 and 1 for the R_{uptake} calculation. The ambient $OH_{(g)}$ concentration is mainly driven by daytime photochemical process, with global tropospheric average $OH_{(g)}$ of ~1.09×10^6 molec cm^{-3} (14). We calculated R_{uptake} by assuming $OH_{(g)}$ concentrations of 5×10^4, 2×10^5 to 1×10^6 molec cm^{-3}. The nighttime $OH_{(g)}$ is mainly produced from ozonolysis of alkenes (15, 16). Holland et al. (17) found that the nighttime $OH_{(g)}$ was generally below the instrument detection limit, and they estimated an upper limit of 5×10^4 molec cm^{-3} as the average nighttime $OH_{(g)}$. A comparison of the OH production rate due to the gas-to-droplet OH uptake and spontaneous OH production at the interface suggests that the interfacial $OH_{(aq)}$ production may dominate over R_{uptake} at nighttime (see **Fig. 4**), which also highlights the importance of this interfacial chemistry in driving aqueous aerosol and cloud oxidation at nocturnal atmosphere. Note that our R_{uptake} calculation represents the maximum OH uptake rate, as the liquid-to-gas transfer process is not considered.

Text S12 Bulk production of $OH_{(aq)}$ radicals from previous studies

The bulk production of $OH_{(aq)}$ radicals was mainly driven by photochemistry and Fenton chemistry, including the photolysis of H_2O_2, NO_3^-, NO_2^- and $Fe(OH)_2^+$ as well as Fenton and photo-Fenton reactions, and the $OH_{(aq)}$ bulk production rates largely depended on the concentrations of $OH_{(aq)}$ precursors (19). There are several studies (18-23) that collected authentic aerosols, cloud and fog water samples from various locations worldwide, and then determined the photochemical $OH_{(aq)}$ production rates through laboratory studies in combination with chemical composition analysis. Faust and Allen (18) reported the first $OH_{(aq)}$ bulk production rate of authentic cloud and/or fog water collected in U.S., which ranged from 8.89×10^{-11} to 8.33×10^{-10} M s^{-1} with an average of 4.37×10^{-10} M s^{-1} (n=4). Arakaki and Faust (23) collected authentic continental cloud waters from Whiteface Mountain, New York, and they determined an average $OH_{(aq)}$ photoproduction rate of 1.81×10^{-10} M s^{-1} (n=25). Anastasio and McGregor (19) characterized the aqueous-phase photo-formation of OH radical from winter fog waters collected in Davis, California, resulting in an average $OH_{(aq)}$ bulk production rate of 9.17×10^{-10} M s^{-1} (n=9). Arakakia et al. (20) collected bulk aerosol

samples in Okinawa, Japan, and they reported the average $OH_{(aq)}$ photochemical formation rate of 1.83×10^{-10} M s^{-1} (n=14) from aqueous extracts of aerosol particle. Bianco et al. (21) collected cloud water at the top of Puy de Dôme station (1465 m a.s.l.) in France, and they experimentally determined total $OH_{(aq)}$ formation rates ranging from 2×10^{-11} to 4×10^{-10} M s^{-1}, with an average of 9.07×10^{-11} M s^{-1} (n=36). Kaur and Anastasio (22) collected fog waters from Davis, California and Baton Rouge, Louisiana, and they determined an average $OH_{(aq)}$ photochemical production rate of 3.33×10^{-10} M s^{-1} (n=8). In summary, based on to the above literature reports, the $OH_{(aq)}$ bulk production rates for authentic aerosol, cloud and fog water generally lie within the range 10^{-10}–10^{-9} M s^{-1}.

Table S1 Summary of chamber aerosol residence time, median aerosol size and mass concentrations (average from SMPS measurements during filter sampling period with assumed density of 1 g cm^{-3}), $[TAOH_{meas}]/[TA_{meas}]$ in filter extracts, $[TAOH_{in\ aerosol}]/[TA_{in\ aerosol}]$ and TAOH production rate (*P*(TAOH)) in aerosol droplets for each filter. All filter extracts (n=46) were analyzed by fluorescence spectrometry for $[TAOH_{meas}]$ (**Text S2**), and some of filter extracts (n=17) were also analyzed by UHPLC-HRMS for $[TA_{meas}]$ (**Text S7**).

Expt ID	Filter ID	Res. time	Median size	Aerosol conc.	$[TAOH_{meas}]$	$[TAOH_{in\ aerosol}]$		*P*(TAOH) in aerosol droplets		$[TA_{meas}]$	$[TA_{in\ aerosol}]$	Experiment description
		min	nm	μg m^{-3}	nM	mM		μM min^{-1}		μM	mM	
E1	filter1	104.5	248	3042.4	357.3	1.53	1.32±0.42 (n=13)	14.6	9.6±8.4 (n=13)	76.8	328.6	1mM TA+25mM NH_4Cl (pH 6.5)
	filter2	176.5	303	1563.5	193.3	1.74		9.9		44.2	398.4	
	filter3	241	319	881.3	91.2	1.57		6.5		26.8	459.0	
	filter4	306.5	329	493.3	43.3	1.13		3.7		N.A.	N.A.	
	filter5	370.5	332	275.3	27.8	1.55		4.2		N.A.	N.A.	
E2	filter1	65	163	2564.6	392.1	2.30		35.3		55.2	323.2	1mM TA+25mM NH_4Cl (pH 6.5)
	filter2	128	190	1603.9	130.2	1.22		9.5		38.5	360.9	
	filter3	191	194	911.8	77.1	1.27		6.7		24.5	404.3	
	filter4	255.5	185	468.5	29.9	0.89		3.5		N.A.	N.A.	
	filter5	319.5	173	222.3	9.0	0.59		1.8		N.A.	N.A.	
E3	filter1	70.5	131	1387.8	100.7	1.09		15.5		62.6	678.1	1mM TA+25mM NH_4Cl (pH 6.5)
	filter2	133.5	147	595.6	32.3	0.85		6.4		36.7	969.7	
	filter3	196.5	145	192.8	18.2	1.42		7.2		N.A.	N.A.	
E4	filter1	77	180	2939.6	289.9	1.45	2.09±0.52 (n=6)	18.8	10.5±4.0 (n=6)	N.A.	N.A.	1mM TA+25mM NH_4Cl (pH 6.5); adding ~3.5 ppm gas-phase cyclohexane
	filter2	139	210	1910.0	168.0	1.32		9.5		N.A.	N.A.	
	filter3	202	218	1159.5	173.4	2.20		10.9		N.A.	N.A.	
	filter4	264	217	675.4	115.0	2.68		10.1		N.A.	N.A.	
	filter5	327	211	388.8	66.2	2.38		7.3		N.A.	N.A.	
	filter6	389	202	216.8	35.1	2.55		6.5		N.A.	N.A.	
E5	filter1	102	126	1205.5	39.7	0.52	1.12±0.44 (n=3)	5.1	6.7±1.9 (n=3)	N.A.	N.A.	1mM TA+25mM NH_4Cl+10mM 1-butanol (pH 6.5)
	filter2	166	143	510.4	50.0	1.54		9.3		N.A.	N.A.	
	filter3	228	141	156.3	13.2	1.29		5.7		N.A.	N.A.	

Expt ID	Filter ID	Res. time	Median size	Aerosol conc.	[$TAOH_{meas}$]	[$TAOH_{in\ aerosol}$]		*P*(TAOH) in aerosol droplets		[TA_{meas}]	[$TA_{in\ aerosol}$]	Experiment description
E6	filter1	96	185	1379.4	30.5	0.34	0.51±0.13 (n=4)	3.5	2.9±0.5 (n=4)	32.0	356.3	1mM TA+25mM NH_4Cl + 3mM adipic acid (pH 6.6)
	filter2	158	201	743.8	22.0	0.44		2.8		18.6	375.9	
	filter3	220	203	359.4	16.3	0.68		3.1		10.2	424.8	
	filter4	282	201	163.4	6.6	0.59		2.1		5.0	453.2	
E7	filter1	96.5	188	1261.9	10.9	0.14	0.28±0.11 (n=5)	1.4	1.3±0.2 (n=5)	20.3	252.8	1mM TA+25mM NH_4Cl + 10mM adipic acid (pH 6.6)
	filter2	159.5	203	686.8	8.3	0.19		1.2		11.2	251.7	
	filter3	224	207	370.5	7.9	0.33		1.5		6.1	252.8	
	filter4	287.5	211	209.2	4.0	0.30		1.0		3.6	274.1	
	filter5	350	213	118.7	3.3	0.43		1.2		1.8	234.5	
E8	filter1	86.5	173	2381.0	208.1	1.28	1.59±0.71 (n=10)	14.8	7.7±3.1 (n=10)	N.A.	N.A.	1mM TA+25mM NH_4Cl (pH 5.0)
	filter2	148.5	199	1486.5	101.9	1.05		7.1		N.A.	N.A.	
	filter3	211.5	203	857.6	86.2	1.55		7.3		N.A.	N.A.	
	filter4	275.5	199	480.8	68.9	2.20		8.0		N.A.	N.A.	
	filter5	338.5	191	257.4	39.7	2.37		7.0		N.A.	N.A.	
	filter6	412	184	123.4	19.4	1.87		4.6		N.A.	N.A.	
E9	filter1	86	172	1238.5	43.8	0.53		6.2		N.A.	N.A.	1mM TA+25mM NH_4Cl (pH 5.0)
	filter2	149	189	667.0	19.2	0.42		2.8		N.A.	N.A.	
	filter3	213	191	344.7	45.6	2.08		9.8		N.A.	N.A.	
	filter4	276.5	182	146.8	25.6	2.55		9.2		N.A.	N.A.	
E10	filter1	92.5	203	1859.2	22.3	0.19	0.27±0.09 (n=5)	2.0	1.3±0.4 (n=5)	N.A.	N.A.	1mM TA+25mM NH_4Cl (pH 9.0)
	filter2	156.5	227	1105.6	13.1	0.19		1.2		N.A.	N.A.	
	filter3	218.5	237	634.3	9.9	0.24		1.1		N.A.	N.A.	
	filter4	281.5	240	362.8	6.9	0.30		1.1		N.A.	N.A.	
	filter5	344.5	246	216.9	6.1	0.44		1.3		N.A.	N.A.	

Table S2 Summary of the two additional chamber experiments that injecting gas-phase cyclohexane and aerosol droplet (NH_4HSO_4), which was to explore whether interfacial OH radical can induce oxidation chemistry for gas-phase compounds

Expt ID	cyclohexane injected (ppm)	PM injected (μg m^{-3})	light conditions
E11	~0.56	~4.8×10^3	UV irradiation and dark
E12	~1.1	~1.0×10^4	dark only

SI References

1. Saran M & Summer KH (1999) Assaying for hydroxyl radicals: hydroxylated terephthalate is a superior fluorescence marker than hydroxylated benzoate. *Free Radic Res* 31(5):429-436.
2. Charbouillot T*, et al.* (2011) Performance and selectivity of the terephthalic acid probe for OH as a function of temperature, pH and composition of atmospherically relevant aqueous media. *Journal of Photochemistry and Photobiology A: Chemistry* 222(1):70-76.
3. Gonzalez DH, Kuang XM, Scott JA, Rocha GO, & Paulson SE (2018) Terephthalate Probe for Hydroxyl Radicals: Yield of 2-Hydroxyterephthalic Acid and Transition Metal Interference. *Analytical Letters* 51(15):2488-2497.
4. Gligorovski S, Strekowski R, Barbati S, & Vione D (2015) Environmental Implications of Hydroxyl Radicals (•OH). *Chem Rev* 115(24):13051-13092.
5. Dubois C*, et al.* (2021) Decrease in sulfate aerosol light backscattering by reactive uptake of isoprene epoxydiols. *Physical chemistry chemical physics : PCCP* 23(10):5927-5935.
6. Yuan B*, et al.* (2017) Proton-Transfer-Reaction Mass Spectrometry: Applications in Atmospheric Sciences. *Chem Rev* 117(21):13187-13229.
7. Krechmer J*, et al.* (2018) Evaluation of a New Reagent-Ion Source and Focusing Ion-Molecule Reactor for Use in Proton-Transfer-Reaction Mass Spectrometry. *Anal Chem* 90(20):12011-12018.
8. Li H*, et al.* (2020) Terpenes and their oxidation products in the French Landes forest: insights from Vocus PTR-TOF measurements. *Atmospheric Chemistry and Physics* 20(4):1941-1959.
9. Depoorter A, Kalalian C, Emmelin C, Lorentz C, & George C (2021) Indoor heterogeneous photochemistry of furfural drives emissions of nitrous acid. *Indoor Air* 31(3):682-692.
10. Abis L*, et al.* (2021) Measurement report: Biogenic volatile organic compound emission profiles of rapeseed leaf litter and its secondary organic aerosol formation potential. *Atmospheric Chemistry and Physics* 21(16):12613-12629.
11. Ervens B (2003) CAPRAM 2.4 (MODAC mechanism): An extended and condensed tropospheric aqueous phase mechanism and its application. *Journal of Geophysical Research* 108(D14).
12. Khaled A, Zhang M, & Ervens B (2022) The number fraction of iron-containing particles affects OH, HO2 and H2O2 budgets in the atmospheric aqueous phase. *Atmospheric Chemistry and Physics* 22(3):1989-2009.
13. Ivanov AV, Trakhtenberg S, Bertram AK, Gershenzon YM, & Molina MJ (2007) OH, HO2, and Ozone Gaseous Diffusion Coefficients. *The Journal of Physical Chemistry A* 111(9):1632-1637.
14. Li M*, et al.* (2018) Tropospheric OH and stratospheric OH and Cl concentrations determined from CH4, CH3Cl, and SF6 measurements. *npj Climate and Atmospheric Science* 1(1).
15. Brown SS & Stutz J (2012) Nighttime radical observations and chemistry. *Chem Soc Rev* 41(19):6405-6447.
16. Geyer A (2003) Nighttime formation of peroxy and hydroxyl radicals during the BERLIOZ

campaign: Observations and modeling studies. *Journal of Geophysical Research* 108(D4).
17. Holland F (2003) Measurements of OH and HO2 radical concentrations and photolysis frequencies during BERLIOZ. *Journal of Geophysical Research* 108(D4).
18. Faust BC & Allen JM (1993) Aqueous-phase photochemical formation of hydroxyl radical in authentic cloudwaters and fogwaters. *Environmental science & technology* 27(6):1221-1224.
19. Anastasio C & McGregor KG (2001) Chemistry of fog waters in California's Central Valley: 1. In situ photoformation of hydroxyl radical and singlet molecular oxygen. *Atmospheric Environment* 35(6):1079-1089.
20. Arakaki T*, et al.* (2006) Chemical composition and photochemical formation of hydroxyl radicals in aqueous extracts of aerosol particles collected in Okinawa, Japan. *Atmospheric Environment* 40(25):4764-4774.
21. Bianco A*, et al.* (2015) A better understanding of hydroxyl radical photochemical sources in cloud waters collected at the puy de Dôme station – experimental versus modelled formation rates. *Atmospheric Chemistry and Physics* 15(16):9191-9202.
22. Kaur R & Anastasio C (2017) Light absorption and the photoformation of hydroxyl radical and singlet oxygen in fog waters. *Atmospheric Environment* 164:387-397.
23. Arakaki T & Faust BC (1998) Sources, sinks, and mechanisms of hydroxyl radical (•OH) photoproduction and consumption in authentic acidic continental cloud waters from Whiteface Mountain, New York: The role of the Fe(r) (r = II, III) photochemical cycle. *Journal of Geophysical Research: Atmospheres* 103(D3):3487-3504.